



Evidence of the mineral $\text{ZnHAsO}_4 \cdot \text{H}_2\text{O}$, koritnigite, controlling As(V) and Zn(II) solubility in a multi-contaminated soil

Carin Sjöstedt^{a,*}, Åsa Kristofferson^{a,1}, Jon Petter Gustafsson^a, Ann-Sophie Heldele^{a,2}, Vadim Kessler^b, Dan B. Kleja^{a,c}

^a Department of Soil and Environment, Swedish University of Agricultural Sciences, P.O. Box 7014, SE-750 07, Uppsala, Sweden

^b Department of Molecular Sciences, Swedish University of Agricultural Sciences, P.O. Box 7015, SE-750 07, Uppsala, Sweden

^c Swedish Geotechnical Institute, Olaus Magnus väg 35, SE-581 93, Linköping, Sweden

ARTICLE INFO

Editorial handling by Dr. Zimeng Wang

Keywords:

Arsenate
Zinc
Koritnigite
Soil
 μ -EXAFS
 μ -XRF
Geochemical equilibrium modeling

ABSTRACT

Assessing element speciation and solubility control mechanisms in multi-contaminated soils poses great challenges. In this study, we examined the speciation and mechanisms controlling the solubility of As and Zn in a soil historically contaminated with As, Cu, Cr, and Zn salts used for wood preservation. The leaching behavior of dissolved species, particles, and colloids was studied in an irrigation experiment with intact soil columns. Batch experiments were used to study the solubility of dissolved species as a function of pH (2–8). The speciation of As and Zn in bulk soil and leached particles was studied with microscale X-ray fluorescence (μ -XRF) and extended X-ray absorption fine structure (EXAFS) spectroscopy. Chemical speciation and solubility were evaluated by geochemical modelling. μ -XRF of bulk soil and particles showed that As and Zn were correlated in space. Bulk- and μ -EXAFS of As and Zn, in combination with calculated ion activity products of possible As-Zn minerals, suggested a koritnigite ($\text{ZnHAsO}_4 \cdot \text{H}_2\text{O}$) phase controlling the dissolved fraction of As(V) and Zn with an apparent $\log K_{sp}$ of -21.9 ± 0.46 . This phase lowered the solubility of As by almost two orders of magnitude in soil at pH > 5, and could therefore be of great importance at other multi-contaminated sites.

1. Introduction

Arsenic is present in many soils contaminated by industrial activities such as glassworks, mining, and wood impregnation using e.g. chromated copper arsenate and ammoniacal copper zinc arsenate. As a result, arsenic is often found together with other elements, e.g., Cr, Cu, Pb, and Zn (Gräfe et al., 2008a; Morrell et al., 2003; Schultz et al., 2004), which may complicate speciation and the solubility mechanisms governing As leaching. In order to design appropriate remediation actions for multi-contaminated soils, information about speciation and solubility mechanisms is needed. While cationic metals generally have low solubility at high pH, As(V) generally has high solubility at high pH (Gräfe et al., 2008a). A common method for determining As speciation in soils is extended X-ray absorption fine structure (EXAFS) spectroscopy at the As K-edge. This method is element-specific, redox-sensitive, and can detect both minerals and other species, e.g. adsorbed elements in

trace amounts. However, it can be difficult to determine the correct phase solely by bulk EXAFS, since e.g., arsenic can be adsorbed to both iron(III) and aluminum(III) (hydr)oxides, which have similar spectra (Slowey et al., 2007; Tiberg et al., 2020). Arsenic can also be co-adsorbed or precipitated with several metals, and these phases are difficult to distinguish from each other by bulk EXAFS. A useful complementary technique that can map different elements in space on μm scale is microscale X-ray fluorescence (μ -XRF), which has been used successfully for studying As in soils, e.g. (Arai et al., 2006; Voegelin et al., 2007; Gräfe et al., 2008a; Hopp et al., 2008; Langner et al., 2013; Itabashi et al., 2019), due to its suitability for heterogeneous samples. μ -XRF can be coupled with μ -X-ray absorption spectroscopy (μ -XAS) methods to determine element speciation at a certain spot, reducing the uncertainties of the analysis of bulk XAS spectra.

Sorption and/or mineral dissolution processes govern dissolved As, but overall mobilization in soils is also determined by the amount of As

* Corresponding author.

E-mail addresses: carin.sjostedt@slu.se (C. Sjöstedt), asa-k@kemakta.se (Å. Kristofferson), jon-petter.gustafsson@slu.se (J.P. Gustafsson), ann-sophie.heldele@web.de (A.-S. Heldele), vadim.kessler@slu.se (V. Kessler), dan.berggren@slu.se (D.B. Kleja).

¹ Present address: Kemakta Konsult AB, Box 12655, SE-112 93 Stockholm, Sweden.

² Present address: Bavarian Environment Agency, Evaluation of Substances and Chemicals, Office Wielenbach, Demollstr. 31, 82407 Wielenbach, Germany.

<https://doi.org/10.1016/j.apgeochem.2022.105301>

Received 15 October 2021; Received in revised form 11 February 2022; Accepted 6 April 2022

Available online 9 April 2022

0883-2927/© 2022 The Authors. Published by Elsevier Ltd. This is an open access article under the CC BY license (<http://creativecommons.org/licenses/by/4.0/>).

associated with mobile colloids and particles. Some data exist on the amount and composition of particles and colloids leaching from contaminated soils (Slowey et al., 2007; Hu et al., 2008; Fritzsche et al., 2011; Löf et al., 2019), but less information is available on the speciation of colloidal and particulate forms of As (Slowey et al., 2007).

Geochemical equilibrium models can be useful tools for assessing speciation and predicting the truly soluble fraction of elements in soil (Groenberg and Lofts, 2014; Sjöstedt et al., 2018). However, model predictions of dissolved As have previously been shown to be less accurate than those for metal cations, with median log root-mean square error (RMSE) values of 0.9–1.0 for As (Groenberg and Lofts, 2014). Further, in some systems only adsorption to Fe and Al (hydr)oxides is considered, while mineral phases that could be present at elevated concentrations of As are neglected (Groenberg and Lofts, 2014). Information on the solid-phase speciation of elements, obtained with EXAFS, has proven to be valuable in constraining the conditions used in model set-up, resulting in more accurate descriptions of solubility control (Gustafsson et al., 2014; Sjöstedt et al., 2018). To our knowledge, no such combined analysis has been performed for As in historically multi-contaminated soils.

The aim of this study was to determine the mechanisms governing solubility and leaching of As and Zn in soil from a historically contaminated (1941–1952) wood preservation site. Specific objectives were to: i) quantify As and Zn leaching as particles, colloids, and truly dissolved species in an irrigation experiment on intact soil columns; ii) determine As and Zn speciation in soil materials and in particles leached from columns in the irrigation experiment, using both μ -XRF and bulk- and μ -EXAFS; and iii) examine As and Zn solubility control mechanisms in equilibrium batch experiments using geochemical modeling and XAS data.

2. Materials and methods

2.1. Soil sampling and soil characterization

Four intact soil columns (20 cm diameter, 30 cm deep measured from the soil surface) were collected from a site at Åsbro, south-central Sweden, contaminated with As, Cr, Cu, and Zn salts from wood preservation activities in 1941–1952 (Löf et al., 2017). Physical and chemical properties of the soil, and details of analytical methods, are presented in full in Löf et al. (2017) and Sjöstedt et al. (2018), and summarized in Table S1 in Appendix A, Supplementary data.

2.2. Irrigation experiment

The irrigation experiment is described in Löf et al. (2017, 2018) and in Fig. S1. The soil columns were fitted with polyamide cloth (mesh size 50 μ m) at the base and placed in an irrigation chamber at 21 °C. Three different irrigation intensities were simulated (2, 10, and 20 mm h⁻¹) with artificial aerated rainwater (Table S2), creating unsaturated flow. These intensities corresponded to average residence times in the columns of 56, 12, and 5.6 h (Löf et al., 2017). The leachate was filtered producing three different operationally defined size fractions: particles (50–0.45 μ m), colloids (0.45 μ m–10 kDa), and truly dissolved (<10 kDa). Concentrations of elements and organic carbon, and pH, were determined in untreated and filtered fractions. For the 0.45 μ m filtered solutions from the columns with 2 and 10 mm h⁻¹ irrigation intensities, arsenic III/V speciation was determined using disposable cartridges with aluminosilicate adsorbent (Meng and Wang, 1998). At the end of the irrigation experiment, one column was split into three layers: the organic-rich uppermost layer (0–4 cm), which was discarded, the “top” layer (4–17 cm) and the “bottom” layer (17–30 cm). These layers were homogenized separately and used for batch experiments and X-ray absorption spectroscopy.

2.3. Batch experiments

Batch experiments were performed to evaluate the solubility of As and Zn at seven different pH values ranging from 2.3 to 7.4, and after different equilibrium times (Sjöstedt et al., 2018). Moist soil was added to duplicate centrifuge bottles at a liquid-solid (L/S) ratio of ~20 (air-dried soil basis). A background electrolyte of 0.01 M NaNO₃ was used and the pH value was adjusted with either HNO₃ or NaOH. The samples were then equilibrated in an end-over-end shaker at 21 °C in darkness for 5 days, or for 1, 5, 32, 61, or 90 days (ambient pH) to investigate the kinetics of metal solubilization. The tubes were opened twice a week to aerate the suspensions.

After equilibration, the tubes were centrifuged and the pH was determined on an aliquot of unfiltered supernatant. The remaining supernatant was filtered using a 0.45 μ m membrane syringe and analyzed for chloride and sulfate. One portion of the filtered supernatant was filtered again using 10 kDa ultra-centrifuge filter bottles and analyzed, for total organic carbon (TOC) using a TOC analyzer, and for metals and P using either inductively coupled plasma atomic emission spectroscopy (ICP-AES) or sector field mass spectrometry (ICP-SFMS), depending on concentration.

2.4. Geochemical equilibrium modeling

In a first step, the geochemical equilibrium model Visual MINTEQ (version 3.1) (Gustafsson, 2013) was used to evaluate elemental speciation and possible mineral equilibria (ion activity products) in solutions obtained in the batch experiment (e.g. Kader et al., 2017). All model input values are listed in Table S3a.

In a second step, the solubility of As and Zn in the batch experiment was predicted using Visual MINTEQ, with data on solid organic matter and hydroxide surfaces as input. Oxalate-extractable As and 0.1 M HNO₃-extractable Zn were used as total ‘reactive’ concentrations (Table S3b). For the complete model set-up, see Supplementary data page S6-S13.

2.5. μ -XRF mapping and μ -XAS

μ -XRF mapping and μ -EXAFS on bulk soil samples were performed at the Diamond Light Source, Didcot, UK, at the microfocuss beamline I18. Soil from the bottom layer (17–30 cm) was fixed by: i) embedding in 1 mm thick epoxy resin (Araldite® 502; Sigma-Aldrich), with one map recorded for this sample, or ii) applied as a thin layer on Kapton® tape, for which two maps were recorded. Using a 10 K LHe cryostat, data were recorded above the As K-edge for As, Ca, Cr, Cu, Fe, Mn, and Zn. The maps were 1 × 1 mm in size, with the pixel size set at 10 × 10 μ m, using a beam size of 2 μ m. μ -EXAFS spectroscopy at the As and Zn K-edges was performed for four hotspots (three with both As and Zn, one with Zn) on one of the Kapton® tape maps, using a beam size of approximately 30–40 μ m. Between 5 and 14 scans were collected. A gold foil at 11919 eV was used as an energy reference.

μ -XRF mapping on particles isolated from leachate in the 20 mm h⁻¹ irrigation treatment was performed at Stanford Synchrotron Radiation Lightsource (SSRL), Menlo Park, California, USA, at beamline 2-3. Particles were isolated by filtration through a 0.45 μ m polyvinylidene fluoride filter (Durapore) in a 142 mm polycarbonate in-line sample holder. The filter was placed on the sample holder with the particle side facing the beam, under ambient temperature and air. The map was recorded at 12000 eV (above the As K-edge) with a dwell time of 25 ms, mapping As, Ca, Cr, Cu, Fe, Mn, and Zn. The map size was 1.65 × 1.22 mm and the pixel/beam size was 2 × 2 μ m. Microscale X-ray absorption near edge structure spectroscopy (μ -XANES) at the Zn K-edge was performed for one hotspot (one scan).

2.6. Bulk EXAFS

Bulk As K-edge EXAFS spectra of soil and particles from the irrigation experiment were recorded at beamline I811 at the MAX-lab synchrotron, Lund University, Sweden. The beamline was equipped with a Si[111] double crystal monochromator. The storage ring was operated at 1.5 GeV with a maximum current of 250 mA. The scans were collected at ambient room temperature and air in fluorescence mode using a passivated implanted planar silicon (PIPS) detector with a Ge filter. Higher-order harmonics were reduced by detuning the second monochromator crystal to reflect 20% of maximum intensity at the end of the scan. A reference sample of elemental arsenic ($E_0 = 11867$ eV), diluted in boron nitride, was run simultaneously with the samples. Six scans were collected for each sample. Bulk soil samples (<2 mm) from the top and bottom layer were applied with Kapton tape. Particles on the 0.45 μm polyvinylidene fluoride filter from the 10 mm h^{-1} were also run.

Bulk Zn K-edge EXAFS spectra were recorded for the bottom soil sample at beamline 4-1 at SSRL. The beamline was equipped with a Si [220] monochromator at $\Phi = 90^\circ$. All scans were collected at 80 K (LN_2) using a 32-element Ge detector in fluorescence mode. A Cu 3λ -filter, Al foil, and 2.8 mm Soller slits were used. Higher-order harmonics were reduced by detuning the second monochromator crystal to reflect 30% of maximum intensity at the end of the scan. A reference sample of Zn foil, $E_0 = 9659$ eV, was run simultaneously with the samples. Four scans were collected. EXAFS standards are listed in Table S4. We recorded a Zn K-edge spectrum of a koritnigite mineral sample from the Svornost mine in Jachymov, Czech Republic (Table S4 and Figs. S2–S5 for more details).

2.7. EXAFS data evaluation

EXAFS data interpretation was performed using the Demeter software package, version 0.9.24, which includes Athena and Artemis while using Ifeffit 1.2.11 (Ravel and Newville, 2005), Atoms (Ravel, 2001), and Feff (Rehr et al., 2009). Raw spectra were averaged and deglitched using Athena when needed. A spline using the Autobk function was used to extract the EXAFS function, with an rbk parameter set to 0.85 for As and to 1.0 for Zn. Depending on data quality, Fourier transform (FT) was made using a Hanning window between appropriate k -ranges. Using Artemis software, the data were fitted between 0.85 and 4 \AA for As and between 1 and 4 \AA for Zn in k -weights 1, 2, and 3 simultaneously, using

different Feff paths from the model compounds. Shell fitting was performed with parameters as described in Table S5 (As) and S6 (Zn). Linear combination fitting (LCF) was also performed on the k^3 -weighted As and Zn K-edge EXAFS spectra between 3.6 and 10.5 \AA^{-1} (As) and between 2 and 10 \AA^{-1} (Zn), and of the Zn XANES (further details in SI page S16).

3. Results and discussion

3.1. Irrigation experiment

Most of the leached As was truly dissolved, with 0–22% leached as particles and 1.5–6.7% as colloids at all three irrigation intensities (Fig. 1). Arsenic speciation made on column leachates (<0.45 μm) at both the 2 mm h^{-1} ($n = 4$) and 10 mm h^{-1} ($n = 4$) irrigation intensities confirmed that a major fraction of dissolved As ($>95\%$) was present as As(V). For Zn, a larger fraction was leached as particles (1.2–58%) and colloids (3.8–29.7%) at the three irrigation intensities (Fig. 1). There was no clear effect of irrigation rate on leaching of particulate and colloid-bound As and Zn. However, both elements showed a decreasing trend in particulate concentrations over time at all three irrigation intensities, probably owing to depletion of particles over time during the experiment (Löv et al., 2018). A major fraction of Fe (89–96%) was found in the particulate fraction (Fig. 1). A previous study (Löv et al., 2017) using EXAFS spectroscopy found that Fe in particles and colloids comprised a mixture of ferrihydrite and Fe(III) in association with organic matter.

The concentration of truly dissolved As and Zn (<10 kD) decreased slightly with increasing irrigation, with a significant difference ($p < 0.05$) between the final measurements at all three intensities for As, and for Zn except between 10 and 20 mm h^{-1} , indicating kinetically constrained dissolution of As- and Zn-bearing solid phases (Fig. 1, Fig. S6). The irrigation intensities corresponded to contact times of 6, 12, and 56 h (Löv et al., 2017).

3.2. Batch experiments and IAP calculations

The duplicates were very similar to each other (Table S3a), and therefore averages are occasionally reported. Dissolved As and Zn reached equilibrium after ≤ 5 days at ambient pH (Fig. S6). Somewhat unexpectedly, the batch experiments showed the lowest dissolved As

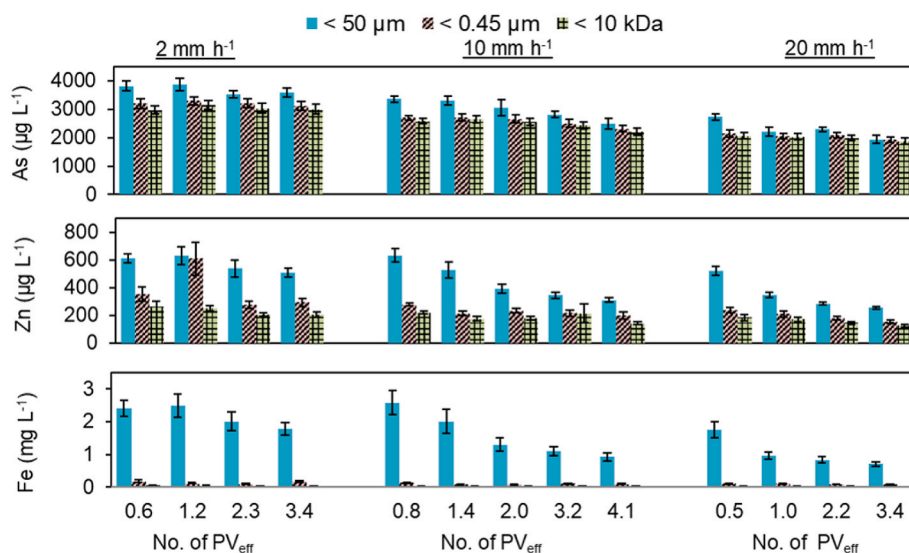
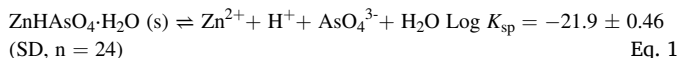


Fig. 1. Concentrations of As, Zn, and Fe as a function of effective pore volume (PV_{eff}) during the irrigation experiment. Average values for four columns are displayed, with error bars indicating standard error of the mean. Data for As and Zn (2 mm h^{-1}) (Löv et al., 2019) and Fe (Löv et al., 2017) have previously been reported.

concentrations to occur in the pH range 6–7 (Fig. 2a). The solubility of As(V) is normally thought to be dominated by sorption by Al and/or Fe (hydr)oxides, resulting in the strongest binding at low pH values (Goldberg, 1986). By contrast, Zn showed the expected trend of lowest solubility at the highest pH value, while all geochemically active Zn was dissolved at the two lowest pH values (Fig. 2b).

From the μ -XRF results it was clear that As and Zn were spatially correlated (c.f. section 3.3). An independent evaluation of the presence of a possible As- and Zn- containing mineral in the test soil was made by calculating the IAP for several As- and Zn-containing minerals using the dissolved phase from the batch experiment (duplicates) (Fig. 3, Table S7). Note that five days of equilibration were used in the acid-base titration experiment, but only minor changes in saturation indices were observed for equilibrium times as long as 90 days for the ambient pH (Figs. 3 and S6, Table S7). Few minerals were supersaturated at any pH value and, for those that were, the IAP varied substantially over the pH range investigated and did not match the measured solubility (Fig. 3, Table S7). The mineral phases showing the most consistent IAP values were phases having a ZnHAsO_4 composition. The only ZnHAsO_4 mineral phase that we were able to find in the literature is $\text{ZnHAsO}_4 \cdot \text{H}_2\text{O}$, koritigite, but unfortunately, no solubility product of this phase has been reported in the literature. The apparent average log IAP from our data was:



3.3. μ -XRF mapping

The epoxy-treated soil sample was found to contain As(III). This was very likely an artefact, since bulk EXAFS of non-epoxy-treated bulk soil showed only As(V) (section 3.4). However, the epoxy-treated sample was physically stable under the beam and could therefore be used for spatial correlation analysis. Arsenic was most strongly correlated with Zn in all three maps, with R^2 -values of 0.69–0.85 (Fig. 4a and b, Figs. S7 and S8 in SI). Interestingly, As showed no correlation with Fe ($R^2 < 0.15$).

In the particulate sample collected from the irrigation experiment (at 20 mm h^{-1}), As and Zn were again correlated ($R^2 = 0.40$) (Fig. 4c, Fig. S9). However, in contrast to the bulk soil, there was also a strong correlation between As and Fe in this sample ($R^2 = 0.48$).

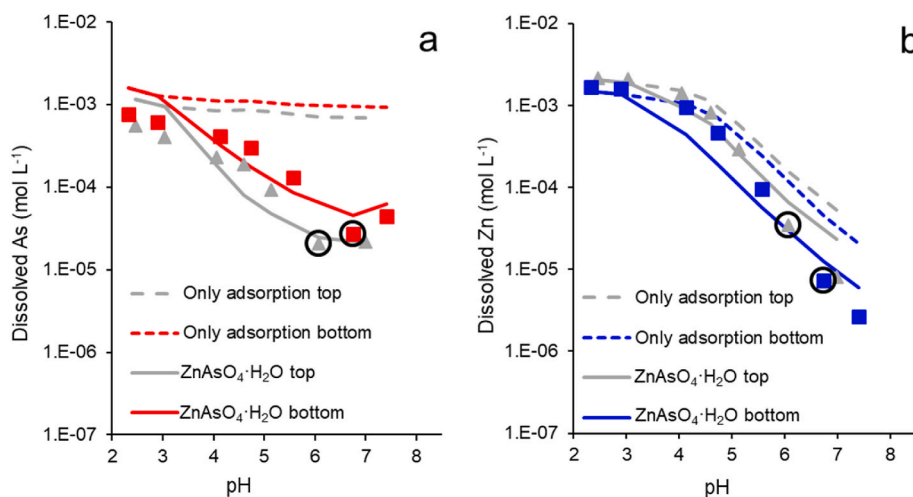


Fig. 2. Solubility of (a) As and (b) Zn at different pH values filtered through <10 kDa filters (symbols) (averages). Grey triangles denote top and colored squares bottom soil layer and black circles ambient pH. Geochemical modeling with only adsorption to oxides and solid organic matter (SOM) are shown with striped lines, whereas full lines denote precipitation of $\text{ZnHAsO}_4 \cdot \text{H}_2\text{O}$ with our log solubility product of -21.9 .

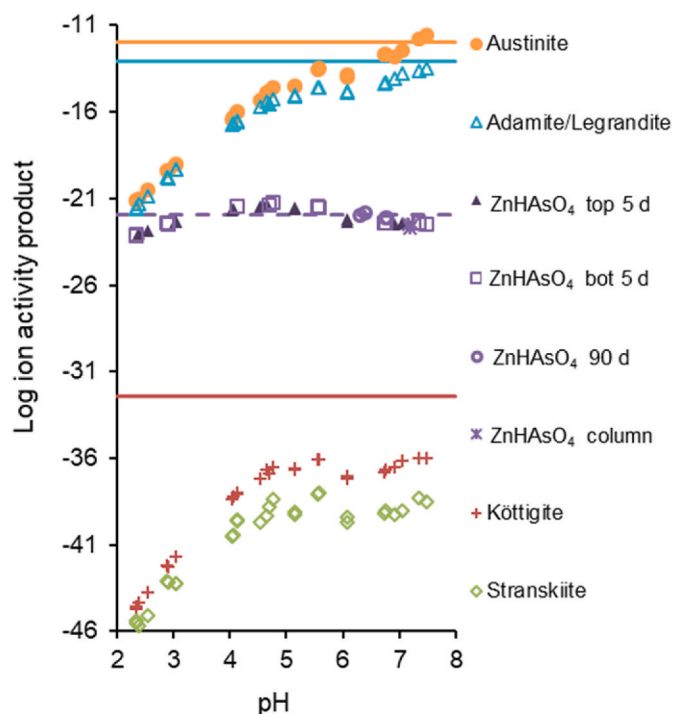


Fig. 3. Measured log ion activity products of various As-Zn minerals in the 5 days batch experiments top and bottom layer, duplicates, (symbols) compared to log solubility products (lines) when present in the literature. For ZnHAsO_4 , results from 90 days batch (ambient pH) and column experiments are also given (symbols), and our apparent log solubility product of -21.9 ± 0.46 (SD) (striped lines).

3.4. As and Zn XAS

μ -EXAFS spectra were recorded on four hotspots (Fig. 4b), where hotspots 1–3 contained both As and Zn and hotspot 4 was dominated by Zn. The intensities of the elements are listed in Table S8. Hotspots 1 and 2 contained mainly As and Zn, whereas hotspot 3 had a 10-fold stronger signal of Fe and less Zn than hotspots 1 and 2. The EXAFS spectra and the magnitude of Fourier transform for As and Zn are shown in Fig. 5, the shell-fitted parameters in Table S5 (As) and Table S6 (Zn), whereas the LCF results are shown in Fig. S10 and Table S9 (As K-edge EXAFS),

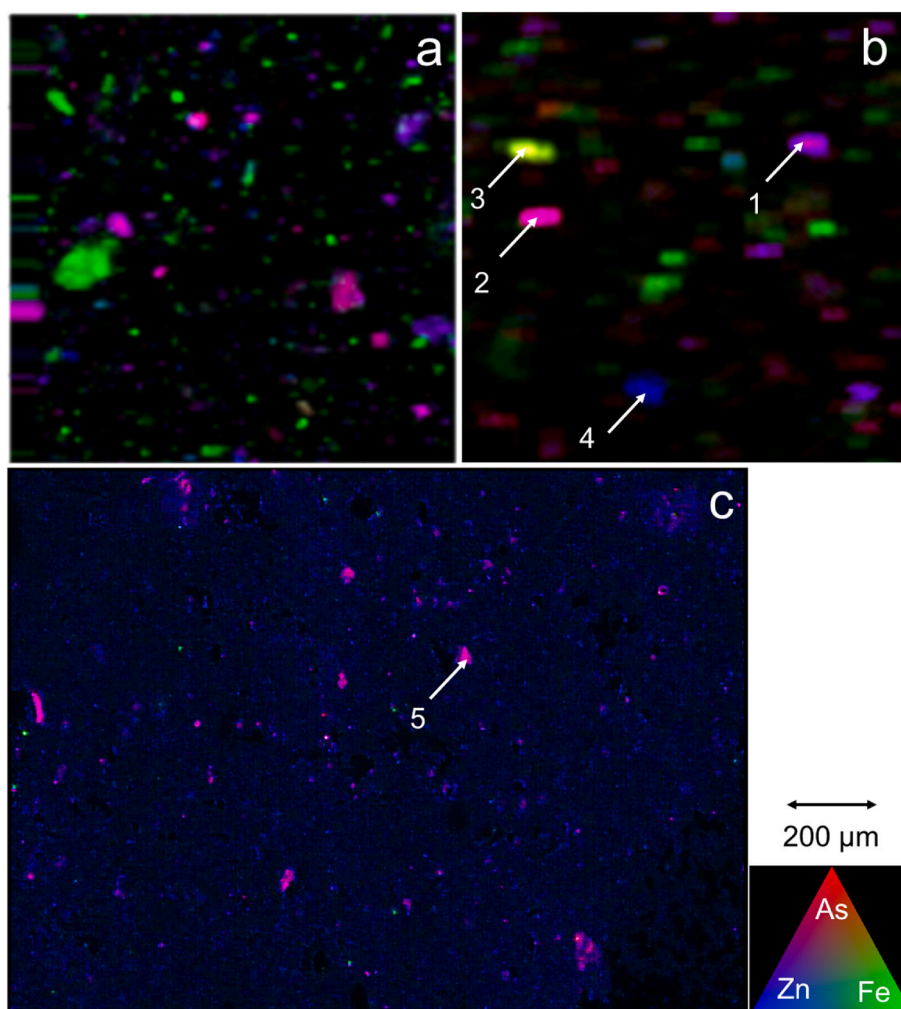


Fig. 4. μ -XRF maps of the bottom soil sample (a) epoxy-treated and (b) with Kapton tape. (c) Map of the particle sample from the irrigation experiment. Numbers 1–5 in (b) and (c) refer to μ -EXAFS of hotspots of As (1–3) and Zn (1–5).

Fig. S11 and **Table S10** (Zn K-edge EXAFS), and **Fig. S12** and **Table S11** (Zn K-edge XANES). Three different As species and three different Zn species were detected in the hotspots, indicating considerable spatial heterogeneity of As and Zn speciation in the soil (**Fig. 4b**). However, As was present as As(V) in all samples, based on As–O distances of 1.69–1.72 Å (**Mähler et al., 2013**). The As and Zn spectra for each hotspot are evaluated in more detail below.

The second shell of the As K-edge EXAFS spectra of hotspot 1 in **Fig. 4b** fitted a model with average As...Zn distance 3.38 Å (**Fig. 5a** and **b**, **Table S5**). This distance occurs in many minerals that contain As and Zn (**Table S5**), but the spectrum did not resemble adamite or ojuelaite (from **Gräfe and Sparks, 2005**). Paradamite has shorter As...Zn distances (3.11–3.21 Å) (**Bennet, 1980**), which were not found, so it can also be eliminated (**Gräfe and Sparks, 2005**). Legrandite (**Hawthorne et al., 2013**), köttigite (**Hill, 1979**), and koritnigite (**Keller et al., 1980**) are possible mineral phases, but As EXAFS spectra of these are lacking in the literature. Based on the log IAP measurements (section 3.2), legrandite and köttigite are not stable, while the data supported a koritnigite phase. The As spectrum also fitted well with the structure of koritnigite ($\text{ZnHAsO}_4 \cdot \text{H}_2\text{O}$), in which 4.5 Zn distances between 3.30 and 3.50 Å are present according to Feff calculations on the structure determined by **Keller et al. (1980)** (**Table S5**). The Zn K-edge EXAFS spectrum for hotspot 1 was similar to the koritnigite spectrum, except in the k -range region 6.5–8 Å⁻¹ (**Fig. S13a**). The FT was similar also to $R = 3.2$ Å, but above that the koritnigite sample had features which were lacking in hotspot 1 (**Fig. S13b**). It was possible to fit the Zn–O shell with 5.2

oxygens at an average distance of 2.05 Å, similarly as in the koritnigite standard (**Table S6**). A second shell of 0.5 Zn...Zn distance at 3.12 Å could also be fitted in hotspot 1, in accordance with koritnigite, which was fitted with 0.5 Zn...Zn distance at 3.14 Å. Koritnigite also have 1.5 Zn distances at 3.25 Å and 4.5 As distances between 3.30 and 3.50 Å according to Feff calculations, but due to the waves cancelling each other it was not possible to fit these distances, either in the koritnigite standard or the hotspot 1. **Gräfe and Sparks (2005)** also noted that the waves cancelled each other and that the amplitude was reduced in Zn–As mineral spectra. However, the koritnigite spectrum could be fitted with 0.5 As distance at 3.73 Å, 1 Zn distance at 4.64 Å, and 1.5 Zn at 5.11 Å, in accordance with the Feff calculations, but these distances were not possible to fit in the hotspot 1, probably due to the sample being less long-range ordered (**Table S6**). The XANES spectrum resembled koritnigite with a white line at 9669 eV and a shoulder at 9666 eV (**Fig. S12**) and according to LCF 50% was koritnigite (**Table S11**). In summary, a koritnigite-like phase in hotspot 1 was supported by both As and Zn μ -EXAFS/XANES.

Hotspot 2 (see **Fig. 4b**) mainly had As and Zn, but also some Cr (**Table S8**). The second shell of the As spectra was best fitted with As...Zn/Fe paths at 2.90 Å and at 3.28 Å in the second shell (**Fig. 5a** and **b**, **Table S5**). The Zn second shell could be fitted with a Zn...Zn/Fe distance of 3.20 Å, but not with a Zn...As distance of 2.90 Å, suggesting that this distance found in the As EXAFS is to another metal, such as Fe. The As spectrum had similar paths to those in a sample with As and Zn co-adsorbed to goethite from (**Gräfe et al., 2008b**). The Zn spectrum of

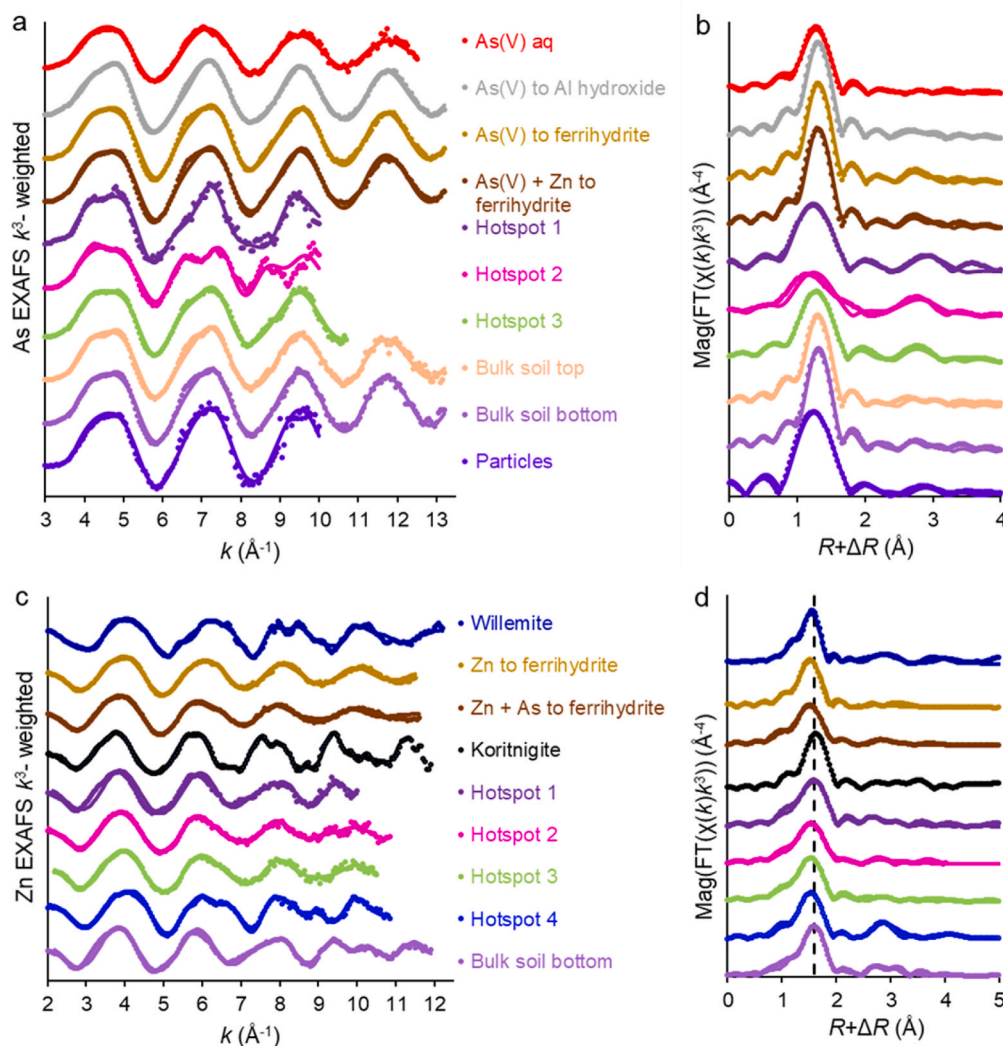


Fig. 5. (a) Arsenic K-edge k^3 -weighted EXAFS, (b) As magnitude of Fourier transform (FT), (c) Zn K-edge k^3 -weighted EXAFS, and (d) Zn magnitude of FT. Dots are data and lines shell model fits.

hotspot 2 resembled our standard, where Zn and As were co-adsorbed to ferrihydrite (Fig. 5c and d and LCF results in Table S10 in Supplementary data). Therefore, it is likely that As and Zn were adsorbed to ferrihydrite or goethite at hotspot 2. The As spectrum did not resemble ojuelaite and the Zn spectrum did not resemble adamite (Gräfe and Sparks, 2005). Further, none of the other minerals listed in Table S5 contains an As...Fe/Zn distance of 2.90 \AA , so they can also be rejected.

Hotspot 3 had a 10-fold stronger Fe signal, but a weaker Zn signal, than hotspots 1 and 2 (Table S8). The As EXAFS spectrum resembled our standard with As(V) adsorbed to ferrihydrite (Fig. 5a and b, LCF results in Table S9) and an As...Fe/Zn path at 3.32–3.35 \AA could accordingly be fitted (Table S5). The Zn EXAFS spectrum resembled Zn adsorbed to ferrihydrite (Fig. 5c and d, see LCF results in Table S10), with a first Zn-O shell at 2.00 \AA and a second shell with a Zn...Fe/Zn path at 3.21 \AA (Table S6). This suggests that both As and Zn were adsorbed to ferrihydrite at hotspot 3.

Hotspot 4 consisted mainly of Zn, with little of the other recorded elements (Table S8), but lighter elements such as Al, Si, P, C, and O may have been present. It was possible to fit the EXAFS spectrum with Zn-O paths at 1.98 \AA , suggesting tetrahedral coordination in the first shell (Waychunas et al., 2002), and Zn...Zn paths at 3.25 \AA and 4.57 \AA (Fig. 5c and d, Table S6). This excludes the phases Zn adsorbed to γ -alumina and Zn-Al layered double hydroxide (LDH) (Wang et al., 2017; Gou et al., 2018). According to the LCF of both EXAFS and XANES spectra, hotspot

4 resembled willemite (Medas et al., 2014) to about 47–65% (Tables S10 and S11) and also in the R and CN parameters (Table S6), but other forms are also possible.

In summary, hotspot 1 contained an As- and Zn-containing mineral, probably short-range ordered koritnigite, whereas hotspots 2 and 3 most likely dominated by As and Zn adsorbed to ferrihydrite, with As present in two different forms. Hotspot 4 consisted of a Zn-containing compound, which could not be identified.

The bulk EXAFS spectra provided data on the phase identified by μ -EXAFS that dominated in the soil. The LCF of the As EXAFS bulk spectra of the top and bottom layer of the bulk soil showed that As adsorbed to (hydr)oxides dominated, whereas up to 24% could be fitted as hotspot 1 (Table S9 and Fig. S10). It was possible to fit As...Zn/Fe distances of on average 3.37–3.39 \AA , which lie between the distances in As(V) adsorbed to ferrihydrite and koritnigite (Table S5). The bulk spectra did not resemble hotspot 2, and according to LCF this particular form of As was a minor phase, less than 7% of the bulk soil spectra (Table S9). The Zn K-edge bulk EXAFS spectrum of the bottom sample was very similar to hotspot 1 in k -space and to koritnigite (Figs. S13a and c), and the shell-fitted parameters were also similar (Table S6). This suggests that the speciation of Zn was similar to the one found in hotspot 1, possibly involving a short-range ordered koritnigite phase.

According to LCF, the As EXAFS bulk spectrum of the particles leached from the irrigation experiment resembled As(V) adsorbed to

ferrihydrite to a larger extent than the As-Zn phase of hotspot 1 (Table S9). It was shell-fitted with As...Zn/Fe distances at 3.33–3.36 Å (Table S5), also suggesting a phase similar to As(V) adsorbed to ferrihydrite and hotspot 1 (Fig. 5a and b). The μ -XRF data confirmed that As was spatially correlated with Fe ($R^2 = 0.48$), as well as Zn ($R^2 = 0.40$), in the particle sample (Fig. S5). Unfortunately, Zn bulk EXAFS and μ -EXAFS data were not recorded for the particle sample. However, one Zn K-edge μ -XANES spectrum was recorded for one hotspot (5 in Fig. 4c). The Zn K-edge XANES spectrum resembled koritnigite (Fig. S12) as seen by a small shoulder at 9666–9667 eV and by a sharper and higher white-line maximum at 9669 eV compared with hotspots 2 and 3. This suggests that koritnigite was present also in the particles.

3.5. Geochemical equilibrium modeling

In a final step, the dissolved concentrations of As and Zn obtained in the batch experiment (averages) were predicted using geochemically active concentrations of As and Zn as input to Visual MINTEQ (Table S3b). When the As solubility in the acid-base titration experiment was predicted with only adsorption to ferrihydrite/Al hydroxide, there was a poor fit to the measured dissolved As concentrations (RMSE top = 0.96, bottom = 0.89) (Fig. 2a). When including possible precipitation of mimetite, $Pb_5(AsO_4)_3Cl$ ($\log K_{sp} = -83.53$), which has previously been shown to describe the solubility of Pb^{2+} well in this soil (RMSE top = 0.28, bottom = 0.22) (Sjöstedt et al., 2018), the RMSE values for As were still high (0.90 and 0.87 for top and bottom, respectively) (data not shown). Possibly, the pool size of mimetite in the soil was too small to explain the As solubility patterns. This could be explained by the fact that the pool sizes of As were 7- and 14-fold larger than for Pb in the two samples (Table S1). For Zn, the modeling results were also less satisfactory (RMSE = 0.41 and 0.47 for top and bottom, respectively), especially at higher pH values (Fig. 2b) when only adsorption to solid organic matter and hydroxides was considered. In an effort to improve the description of the observed As and Zn solubility, koritnigite was added to Visual MINTEQ as a possible phase, with $\log K_{sp} = -21.9$, based on the apparent average log IAP values of our study (Table S7). As expected, this improved prediction of the solubility of both As and Zn considerably (Fig. 2). At ambient pH values, 62% of the solid-phase As was estimated to be present as koritnigite in both the top and bottom layer. According to the model, the remaining As was adsorbed to ferrihydrite and Al hydroxide, which is in fair agreement with the EXAFS results (section 3.4). For Zn at ambient pH, 40% (top) and 64% (bottom) was predicted as being koritnigite. Further, 60% (top) and 36% (bottom) was predicted to be Zn sorbed to solid organic matter. This is in fair agreement with the EXAFS results (section 3.4), which suggested that a mineral phase with a koritnigite structure dominated Zn speciation in the bottom layer. Zinc adsorbed to organic matter might be present in small concentrations in the test soil. It is difficult to detect this using EXAFS spectroscopy, since it gives a small contribution to the second shell due to the light backscatter of carbon (Karlsson and Skyllberg, 2007).

3.6. Conclusions

The irrigation experiment demonstrated that most of the As was mobilized in the truly dissolved fraction (on average 84%), whereas for Zn the corresponding percentage was lower (on average 33%). The remaining fraction was mainly particles ($>0.45 \mu m$), which contained koritnigite in association with iron (hydr)oxides as well as As(V) adsorbed by iron (hydr)oxides. In the soil, koritnigite was identified as a separate phase, not associated with iron(hydr)oxides. The solubility of As was governed by this mineral phase (apparent log solubility product of -21.9), which lowered the solubility by two orders of magnitude, compared to a situation where adsorption by iron (hydr)hydroxides controls the solubility.

3.7. Environmental implication

Our results strongly indicated the presence of koritnigite in the soil and it is suggested that this mineral governed the solubility of As and Zn in a wide pH range (4.0–7.4). This rare mineral has previously been reported in the metal deposit Tsumeb in Namibia (Keller et al., 1979) and as a Co- and Ni-rich variety in the Jáchymov ore district, Czech Republic (Schmetzer et al., 1980). Gräfe and Sparks (2005) reacted $250 \mu mol L^{-1} AsO_4$ and $250 \mu mol Zn$ with 10 ppm goethite at pH 7, and observed a koritnigite-like phase after six months of aging. They received a log IAP of -20.7 at pH 7 for koritnigite, as compared to our apparent average log solubility product of -21.9 ± 0.43 (SD). Judging from their and our results it seems clear that a koritnigite phase can form when high arsenate and Zn concentrations are present at near-neutral pH. In the study by Gräfe and Sparks (2005) goethite was required for koritnigite to form, since when they performed a similar experiment without goethite, a köttigite structure was formed instead. Our study confirmed the interaction between As, Zn, and Fe in the particulate fraction in leachate. In the soil samples, As and Zn were not associated with Fe, but koritnigite could apparently still be formed.

The presence of koritnigite as a stable phase in multi-metal-contaminated soils can reduce the soluble concentrations of As and Zn significantly compared to a situation where their solubility is being controlled by adsorption processes. Future studies of As and Zn at multi-contaminated sites should consider the possibility of formation of koritnigite and its potential role in governing mobilization of As.

Funding

This work was supported by the Swedish Research Council for Environment, Agricultural Sciences and Spatial Planning (FORMAS) (No. 219-2012-868). The work was carried out with the support of the Diamond Light Source, instrument I18 (proposal SP16025). Parts of this research were carried out at beamline I811, MAX-lab synchrotron radiation source, Lund University, Sweden. Funding for the beamline I811 project was kindly provided by The Swedish Research Council and The Knut och Alice Wallenbergs Stiftelse. Use of the Stanford Synchrotron Radiation Lightsource, SLAC National Accelerator Laboratory, is supported by the U.S. Department of Energy, Office of Science, Office of Basic Energy Sciences, under Contract No. DE-AC02-76SF00515. The funding sources had no involvement on the research performed.

The following people are also gratefully acknowledged: Konstantin Ignatyev for all the help at the Diamond Light source; staff at I811, MAX-lab, for help at the beamline; Courtney Roach at SSRL for all the help; Vincent Noel and Kristin Boye at SSRL for running the koritnigite EXAFS standard at their beamtime, and Charlotta Tiberg, Daniela Medas, Ingmar Persson, and Markus Gräfe for providing EXAFS standards. Mary McAfee for language checking.

Declaration of competing interest

The authors declare that they have no known competing financial interests or personal relationships that could have appeared to influence the work reported in this paper.

Appendix A. Supplementary data

Supplementary data to this article can be found online at <https://doi.org/10.1016/j.apgeochem.2022.105301>.

References

- Arai, Y., Lanzirotti, A., Sutton, S.R., Newville, M., Dyer, J., Sparks, D., 2006. Spatial and temporal variability of arsenic solid-state speciation in historically lead arsenate contaminated soils. *Environ. Sci. Technol.* 40, 673–679. <https://doi.org/10.1021/es051266e>.
- Bennet, T.J., 1980. Crystal structure of paradamite. *Am. Mineral.* 65, 353–354.

- Fritzsche, A., Rennert, T., Totsche, K.U., 2011. Arsenic strongly associates with ferrihydrite colloids formed in a soil effluent. *Environ. Pollut.* 159, 1398–1405. <https://doi.org/10.1016/j.envpol.2011.01.001>.
- Gou, W., Siebecker, M.G., Wang, Z., Li, W., 2018. Competitive sorption of Ni and Zn at the aluminum oxide/water interface: an XAFS study. *Geochem. Trans.* 19 (9) <https://doi.org/10.1186/s12932-018-0054-7>.
- Goldberg, S., 1986. Chemical modeling of arsenate adsorption on aluminum and iron oxide minerals. *Soil Sci. Soc. Am. J.* 50, 1154–1157. <https://doi.org/10.2136/sssaj1986.03615995005000050012x>.
- Gräfe, M., Sparks, D.L., 2005. Kinetics of zinc and arsenate co-sorption at the goethite-water interface. *Geochem. Cosmochim. Acta* 69, 4573–4595. <https://doi.org/10.1016/j.gca.2005.04.016>.
- Gräfe, M., Tappero, R.V., Marcus, M.A., Sparks, D.L., 2008a. Arsenic speciation in multiple metal environments II. Microscopic investigation of a CCA contaminated soil. *J. Colloid Interface Sci.* 321, 1–20. <https://doi.org/10.1016/j.jcis.2008.01.033>.
- Gräfe, M., Tappero, R.V., Marcus, M.A., Sparks, D.L., 2008b. Arsenic speciation in multiple metal environments: I. Bulk-XAFS spectroscopy of model and mixed compounds. *J. Colloid Interface Sci.* 320, 383–399. <https://doi.org/10.1016/j.jcis.2008.01.028>.
- Groenenberg, J.E., Lofers, S., 2014. The use of assemblage models to describe trace element partitioning, speciation, and fate: a review. *Environ. Toxicol. Chem.* 33, 2181–2196. <https://doi.org/10.1002/etc.2642>.
- Gustafsson, J.P., 2013. Visual MINTEQ Program Version 3.1. Stockholm, Sweden (accessed April 16, 2020). <https://vminteq.lwr.kth.se/>.
- Gustafsson, J.P., Persson, I., Oromieh, A., Geranmayeh, van Schaik, J.W.J., Sjöstedt, C., Kleja, D.B., 2014. Chromium(III) complexation to natural organic matter: mechanisms and modeling. *Environ. Sci. Technol.* 48, 1753–1761. <https://doi.org/10.1021/es404557e>.
- Hawthorne, F.C., Abdu, Y.A., Tait, K.T., 2013. Hydrogen bonding in the crystal structure of legrandite: $Zn_2(AsO_4)(OH)(H_2O)$. *Can. Mineral.* 51, 233–241. <https://doi.org/10.3749/canmin.51.2.233>.
- Hill, R.J., 1979. The crystal structure of köttigite. *Am. Mineral.* 64, 376–382.
- Hopp, L., Nico, P.S., Marcus, M.A., Peiffer, S., 2008. Arsenic and chromium partitioning in a podzolic soil contaminated by chromated copper arsenate. *Environ. Sci. Technol.* 42, 6481–6486. <https://doi.org/10.1021/es800615f>.
- Hu, S., Chen, X., Shi, J., Chen, Y., Lin, Q., 2008. Particle-facilitated lead and arsenic transport in abandoned mine sites soil influenced by simulated acid rain. *Chemosphere* 71, 2091–2097. <https://doi.org/10.1016/j.chemosphere.2008.01.024>.
- Itabashi, T., Li, J., Hashimoto, Y., Ueshima, M., Sakanakura, H., Yasutaka, T., Imoto, Y., Hosomi, M., 2019. Speciation and fractionation of soil arsenic from natural and anthropogenic sources: chemical extraction, Scanning Electron Microscopy, and micro-XRF/XAFS investigation. *Environ. Sci. Technol.* 53, 14186–14193. <https://doi.org/10.1021/acs.est.9b03864>.
- Kader, M., Lamb, D.T., Wang, L., Megharaj, M., Naidu, R., 2017. Zinc-arsenic interactions in soil: solubility, toxicity and uptake. *Chemosphere* 187, 357–367. <https://doi.org/10.1016/j.chemosphere.2017.08.093>.
- Karlsson, T., Skyllberg, U., 2007. Complexation of zinc in organic soils - EXAFS evidence for sulfur associations. *Environ. Sci. Technol.* 41, 119–124. <https://doi.org/10.1021/es0608803>.
- Keller, P., Hess, H., Süss, P., Schnorrer, G., Dunn, P.J., 1979. Koritnigite, $Zn[H_2O][HOAsO_3]$, ein neues mineral aus Tsumeb, Südwestafrika. *Tschermaks Mineral. Petrogr. Mittl.* 26, 51–58.
- Keller, P., Hess, H., Riffel, H., 1980. Die kristallstruktur von koritnigite, $Zn[H_2O][HOAsO_3]$. *Neues Jahrbuch Mineral., Abhandlungen* 138, 316–332.
- Langner, P., Mikutta, C., Suess, E., Marcus, M.A., Kretschmar, R., 2013. Spatial distribution and speciation of arsenic in peat studied with microfocused X-ray fluorescence spectrometry and X-ray absorption spectroscopy. *Environ. Sci. Technol.* 47, 9706–9714. <https://doi.org/10.1021/es401315e>.
- Löv, Å., Sjöstedt, C., Larsbo, M., Persson, I., Gustafsson, J.P., Cornelis, G., Kleja, D.B., 2017. Solubility and transport of Cr(III) in a historically contaminated soil - evidence of a rapidly reacting dimeric Cr(III) organic matter complex. *Chemosphere* 189, 709–716. <https://doi.org/10.1016/j.chemosphere.2017.09.088>.
- Löv, Å., Cornelis, G., Larsbo, M., Persson, I., Sjöstedt, C., Gustafsson, J.P., Boye, K., Kleja, D.B., 2018. Particle- and colloid-facilitated Pb transport in four historically contaminated soils - speciation and effect of irrigation intensity. *Appl. Geochem.* 96, 327–338. <https://doi.org/10.1016/j.apgeochem.2018.07.012>.
- Lov, Å., Larsbo, M., Sjöstedt, C., Cornelis, G., Gustafsson, J.P., Kleja, D.B., 2019. Evaluating the ability of standardised leaching tests to predict metal(loid) leaching from intact soil columns using size-based elemental fractionation. *Chemosphere* 222, 453–460. <https://doi.org/10.1016/j.chemosphere.2019.01.148>.
- Mahler, J., Persson, I., Herbert, R.B., 2013. Hydration of arsenic oxyacid species. *Dalton Trans.* 42 (5), 1364–1377. <https://doi.org/10.1039/c2dt31906c>.
- Medas, D., Lattanzi, P., Podda, F., Meneghini, C., Trapananti, A., Sprocati, A., Casu, M.A., Musu, E., De Giudici, G., 2014. The amorphous Zn biomineralization at Naracauli stream, Sardinia: electron microscopy and X-ray absorption spectroscopy. *Environ. Sci. Pollut. Res.* 21, 6775–6782. <https://doi.org/10.1007/s11356-013-1886-4>.
- Meng, X., Wang, W., 1998. Speciation of arsenic by disposable cartridges. In: *Book of Posters of the Third International Conference on Arsenic Exposure and Health Effects*. Society of Environmental Geochemistry and Health, University of Colorado at Denver, Denver, CO, 1998.
- Morrell, J.J., Keefe, D., Baileys, R.T., 2003. Copper, zinc, and arsenic in soil surrounding Douglas-fir poles treated with ammoniacal copper zinc arsenate (ACZA). *J. Environ. Qual.* 32, 2095–2099. <https://doi.org/10.2134/jeq2003.2095>.
- Ravel, B., 2001. ATOMS: crystallography for the X-ray absorption spectroscopist. *J. Synchrotron Radiat.* 8, 314–316. <https://doi.org/10.1107/S090904950001493X>.
- Ravel, B., Newville, M., 2005. ATHENA, artemis, hephestus: data analysis for X-ray absorption spectroscopy using IFEFFIT. *J. Synchrotron Radiat.* 12, 537–541. <https://doi.org/10.1107/S0909049505012719>.
- Rehr, J.J., Kas, J.J., Prange, M.P., Sorini, A.P., Takimoto, Y., Vila, F.D., 2009. Ab initio theory and calculations of X-ray spectra. *Compt. Rendus Phys.* 10 (6), 548–559. <https://doi.org/10.1016/j.cry.2008.08.004>.
- Schmetzer, K., Horn, W., Bartelke, W., 1980. Kobalt- und nickel-haltiger koritnigite aus Jáchymov (Joachimsthal), ČSSR – ein zweiter fundpunkt. *Neues Jahrbuch Mineral. Monatsh.* 237–240.
- Schultz, E., Joutti, A., Räsänen, M.-L., Lintinen, P., Martikainen, E., Lehto, O., 2004. Extractability of metals and ecotoxicity of soils from two old wood impregnation sites in Finland. *Sci. Total Environ.* 326, 71–84. <https://doi.org/10.1016/j.scitotenv.2003.12.008>.
- Sjöstedt, C., Löv, Å., Olivecrona, Z., Boye, Kleja, D.B., 2018. Improved geochemical modeling of lead solubility in contaminated soils by considering colloidal fractions and solid phase EXAFS speciation. *Appl. Geochem.* 92, 110–120. <https://doi.org/10.1016/j.apgeochem.2018.01.014>.
- Slowey, A.J., Johnson, S.B., Newville, M., Brown Jr., G.E., 2007. Speciation and colloid transport of arsenic from mine tailings. *Appl. Geochem.* 22, 1884–1898. <https://doi.org/10.1016/j.apgeochem.2007.03.053>.
- Tiberg, C., Sjöstedt, C., Eriksson, A.K., Klysubun, W., Gustafsson, J.P., 2020. Phosphate competition with arsenate on poorly crystalline iron and aluminum (hydr)oxide mixtures. *Chemosphere* 255, 126937. <https://doi.org/10.1016/j.chemosphere.2020.126937>.
- Voegelin, A., Weber, F.-A., Kretschmar, R., 2007. Distribution and speciation of arsenic around roots in a contaminated riparian floodplain soil: micro-XRF element mapping and EXAFS spectroscopy. *Geochem. Cosmochim. Acta* 71, 5804–5820. <https://doi.org/10.1016/j.gca.2007.05.030>.
- Wang, Y.-J., Fan, T.-T., Liu, C., Li, W., Zhu, M.-Q., Fan, J.-X., Gong, H., Zhou, D.-M., Sparks, D.L., 2017. Macroscopic and microscopic investigation of adsorption and precipitation of Zn on γ -alumina in the absence and presence of as. *Chemosphere* 178, 309–316. <https://doi.org/10.1016/j.chemosphere.2017.03.061>.
- Waychunas, G.A., Fuller, C.C., Davis, J.A., 2002. Surface complexation and precipitate geometry for aqueous Zn(II) sorption on ferrihydrite. I: X-ray absorption extended fine structure spectroscopy analysis. *Geochem. Cosmochim. Acta* 66, 1119–1137. [https://doi.org/10.1016/S0016-7037\(01\)00853-5](https://doi.org/10.1016/S0016-7037(01)00853-5).